Gravimetri med treghetssystemer: Oversikt og testresultater

Christian Gerlach, Raul Dorobantu, Christian Ackermann, Narve Kjørsvik og Gerd Boedecker

Vitenskapelig bedømt (refereed) artikkel

Christian Gerlach & al.: Gravimetry with Inertial Navigation Systems: Overview and Test Results

KART OG PLAN, Vol. 70, pp. 46–59. P.O.B. 5003, NO-1432 Ås, ISSN 0047-3278

Today inertial measurement systems are routinely used in navigation applications. The systems determine the acceleration acting on a moving vehicle and by integrating these accelerations twice in time, the travelled distance and thereby the positions along a trajectory can be determined. Before integration of the accelerations, effects due to the gravitational force of the Earth as well as due to apparent forces need to be taken care of, properly. Thereby the gravitational effects are usually taken from models and the apparent forces can be computed from known position and velocity of the vehicle. Instead of using gravity models in navigation applications, one can solve the observation equations for gravity, provided the navigation solution, i.e. the positions, are known. This way, the inertial navigation instrument can be used as a gravimeter on a moving platform – a convenient alternative to airborne (or ship-borne) gravimeters, operationally used today in earth sciences or geophysical exploration. The paper will give a basic overview on the use of inertial sensors for gravimetry and show results achieved during a flight campaign in the German Alps.

Key words: Inertial Navigation Systems, airborne gravimetry, acceleration, gyroscope systems

Christian Gerlach. Associate Professor, Norwegian University of Life and Environmental Sciences (UMB), Institute for Mathematical Sciences and Technology, P.O. Box 5003, NO-1432 Ås. Now at: Bavarian Academy of Sciences and Humanities, Alfons-Goppel-Str. 11, 80539 Munich, Germany. Email: gerlach@bek.badw.de

Sammendrag

Treghetssystemer brukes rutinemessig som et verktøy ved navigasjon. Instrumentene måler akselerasjonene for et fartøy i bevegelse. Målingene inneholder summen av de kinematiske akselerasjonene og gravitasjonen. Posisjoner kan samtidig måles med GPS. Da observeres de ukjente i navigasjonsligningen. Derved har man muligheten til å løse ut gravitasjonen fra navigasjonsligningene. På et fartøy i bevegelse, kan treghetssystemet benyttes som et alternativ til gravimetre ved jordobservasjoner og ved geofysiske undersøkelser.

Artikkelen viser elementært matematisk grunnlag for posisjonering og bestemmelse av gravitasjon ved hjelp av treghetssystemer. Den viser også resultatene fra et eksperiment med flygravimetri brukt i Alpene i Sør-Tyskland.

Gravimetric Geodesy

Gravimetric geodesy deals with the determination of the gravity field of the Earth. Information on the gravity field is important for the realization of a horizontal reference surface and thereby also for the definition of physically relevant heights (like normal or orthometric heights), see e.g. Torge (1991) or Hofmann-Wellenhof and Moritz (2005). The horizontal surface at mean sea level, the *geoid*, is the central quantity desired in gravimetric geodesy. In addition, gravimetric geodesy is important for all studies related to the mass distribution in the earth system, i.e. in geophysics, geophysical exploration and other earth sciences.

Gravity field modelling is based on satellite data for the global, long wavelength structures and terrestrial gravity values for the finer details. Today there are dedicated gravity field satellite missions, like the

US/German GRACE (in orbit since 2002) or ESA's GOCE satellite, launched on March 17, 2009. While GRACE is designed to determine the temporal variations of the geoid over larger areas (several hundred to thousand kilometre resolution, see e.g. Tapley and Reigber, 1999), GOCE will map the fine structure of the static geoid with centimetre precision at a spatial resolution of about 80 km (i.e., the average value of the geoid height over such an area is determined with centimetre precision, see e.g. Rummel et al., 2002 or ESA, 1999). Even smaller details are not visible from satellite data due to the spatial smoothing of the gravity field at orbit height (250 km for GOCE and about 450 km for GRACE). Those smaller details (the fine structure of the geoid) are usually (at least on land) modelled from static terrestrial gravimetry. In contrast to the spatial averages delivered from satellite gravimetry, static terrestrial gravimetry gives point values, which correspond to unfiltered (no spatial averaging) data.

But terrestrial static gravimetry is very costly, i.e. it takes a lot of time to cover a certain area. Therefore airborne methods may be used to cover spatial gaps in an efficient way. This is also important for regions, which are difficult to reach, like the oceans or polar areas. Similar to satellite gravimetry, airborne gravimetry gives values averaged over a certain range (along the flight trajectory), even though with a much higher spatial resolution of some few kilometres only. The spectral content (the smallest spatial feature included in the derived signal) is lowest for satellite gravimetry and highest for terrestrial point values, while airborne gravimetry lays somewhere in between. Combining several data sources in order to determine the best possible gravity field, airborne gravimetry, therefore, does not only cover spatial gaps, but also spectral gaps between the terrestrial point values and the long wavelength features derived from satellites. This way airborne gravimetry strengthens the combination of terrestrial and satellite data.

As will be seen later, data from inertial navigation systems (INS) can be exploited for airborne gravimetry (see e.g., Schwarz, 1983; Schwarz, 1987; Glennie, 1999; Bruton, 2000 or Jekeli and Kwon, 2002) and replace the classical airborne gravimeters. The latter are modified terrestrial gravimeters mounted on a stabilized platform in an aeroplane. But while using an INS might be advantageous both from a theoretical (observation of the full gravity vector is possible) and practical (use of so called *strapdown* systems with easier mechanical setup and smaller size and weight) point of view, the method can still not be seen as operational. After a basic introduction on INS and its use for gravimetry, we will present results from a flight campaign which document the current status of research in airborne gravimetry carried out in the Geomatics group of the Norwegian University of Life Sciences (UMB) in cooperation with the Bavarian Academy of Sciences and Humanities in Munich (BEK) and the Institute for Astronomical and Physical Geodesy (IAPG) at Technische Universität München, Germany.

Navigation and positioning

Navigation basically deals with planning, recording and controlling of the movement of a vehicle (NIMA, 2002). That means it involves (a) planning of the track the vehicle should follow, (b) steady positioning of the vehicle along the track to check the deviations between the real trajectory and the planned route and (c) directing the vehicle such, that it follows the planned route as close as possible. All these tasks are well known to those who use a car navigation system: one enters the point of destination, the system computes the optimal track and guides the driver along the route, while constantly determining the current position. Clearly, one part of navigation is positioning. This is the task geodesists or surveyors are most interested in, while they usually don't care too much for planning and guidance. In this context, the term INS is often meant as a system that computes the trajectory of a vehicle, while it does not consider the additional navigation tasks of planning and guidance. Therefore, strictly speaking, one should talk about the use of inertial *positioning* systems, rather than *navigation* systems. But since the term INS is so common in this

context, we will use it and just keep in mind that we actually deal with positioning only.

Moreover, since the vehicle is moving in space, the task of positioning needs to be extended. For several reasons we might also be interested in the current velocity and the attitude of the vehicle. If we deal with areal photogrammetry, e.g., we need to link the camera frame to an earth fixed frame. The transformation between the two frames involves the attitude angles. Or we might be interested in the velocity in order to take into account velocity induced effects, like, e.g., the Coriolis force. The three quantities position, velocity and attitude describe the state of the vehicle at every epoch, and they are combined into the so called *state vector*. With these three quantities in 3 dimensional space, the state vector consists of 9 elements per epoch. It might well be extended to include also instrumental errors or other parameters, which are estimated along with the actual trajectory. The time series of state vectors per epoch derived from the measurements is called the *navigation solution*.

Principles of positioning

There are several methods for positioning, where one can distinguish between the two basic principles of *position fixing* and *dead reckoning* (see e.g. Hofmann-Wellenhof et al., 2003). In position fixing one always relies on the coordinates of known reference points to determine a new position. The observations between the reference points and the current observation point might, e.g., be directions or distances. In contrast, dead reckoning does not use reference points, but it relies on coordinates which were just estimated along the current trajectory. The technique was traditionally used in marine navigation, where one observed the course of the ship (e.g. with a compass) and its speed in order to determine the position. Continuous observations allowed determination of the ship's trajectory, where each position coordinate depends on those previously determined. A crucial component is the measurement of speed, because it needs to be integrated in time, in order to determine the travelled distance. Thus systematic errors in the observations add up and the position error grows over longer time intervals. This is even more severe for inertial systems, where accelerations are measured instead of speed, thus requiring double integration. Due to this unfavourable error propagation, dead reckoning systems are updated as often as possible, e.g. by position fixing systems, which show more or less constant error behaviour over time (Hofmann-Wellenhof et al., 2003). The Global Positioning System GPS is an example for such a position fixing system, where pseudo-ranges between the user and the GPS satellites (which act as reference points) are observed. Regular GPS updates ensure that the INS derived trajectory does not drift from the true trajectory over the long run. Since the precision over short time intervals is higher for INS, than for GPS, the optimal combination uses a high frequent INS solution (often well above 100 Hz), which is stabilized over longer intervals by GPS data at a much lower sampling frequency (in the range of several seconds down to some few tenth of seconds, depending on receiver and observational setup).

Inertial measurement units

Today many dead reckoning applications in navigation rely on *inertial measurement units* (IMU), carrying two types of sensors which make use of properties of inertia: accelerometers and gyroscopes (see e.g. Jekeli, 2001 or Hofmann-Wellenhof et al., 2003). According to Newton's laws the linear momentum of a mass particle (inertial mass) is constant as long as no forces act on it. In principle, an accelerometer consists of a case, carrying a test mass and the output (measured acceleration) is derived from the relative motion of the mass with respect to the case. The sensor output is called the *specific force* $\boldsymbol{f}$ (bold face letters represent vectors), which is a force per unit mass and therefore is given in units of acceleration. The observation refers to the reference frame of the instrument case, the so called body-frame or *b*-frame. Specifying the reference frame, we use the notation $\boldsymbol{f}^b$ to express that the elements of the vector refer to the *b*-frame.

The kinematic acceleration $\ddot{\boldsymbol{x}}^i$ (second time derivative of position) given in an iner-

tial, non-rotating reference frame (*i*-frame) can be derived as the sum of specific force and Earth's gravitation $\boldsymbol{b}^i$ according to (Jekeli, 2001)

$$\ddot{\boldsymbol{x}}^i = \boldsymbol{f}^i + \boldsymbol{b}^i \tag{1}$$

Equation (1) is called the *equation of motion*. In case, e.g., the instrument was in free fall, the kinematic acceleration equals gravitation and $\boldsymbol{f}^i$ is equal to zero. This is clear from the fact, that both test mass and instrument case fall under the same acceleration (gravitation) and thus there is no relative motion between the two. In fact, the accelerometer senses the reaction force applied to the instrument case (in our free fall example such a reaction force does not exist and the sensor output is zero).

In analogy to the linear momentum, also the angular momentum is constant in inertial space as long as no torque acts on it. Under rotation, the output of the gyroscope is the vector of angular rates (degrees per second) ω_{ib} of the *b*-frame with respect to the *i*-frame.

There are two different types of IMU, namely units mounted on a dynamically stabilized platform and units which are tightly fixed to the vehicle (see e.g. Jekeli, 2001). The latter type is called *strapdown* IMU. The stabilized platforms use the readings from the gyroscopes to mechanically keep the platform in a stable orientation, e.g. always horizontal (so called *local level platforms*). This way, the transformations, necessary to link the sensor readings in the *b*-frame to the navigation frame (*n*-frame) in which the trajectory is computed, are carried out mechanically. Denoting the local level frame as *l*-frame, the *n*-frame and the *l*-frame are identical in case of a local-level stabilized platform. In case of the strapdown systems, where no mechanical stabilization is involved, the same transformations are carried out computationally and the *n*-frame can be chosen arbitrarily by the user. We denote the corresponding transformation matrix from the *b*-frame to the *n*-frame by $\boldsymbol{C}_b^n$.

Due to limitations of mechanical control of stabilized platforms, strapdown systems allow processing of data from much higher dynamic environments, i.e. with faster rotations. Since strapdown instruments follow the motion of the vehicle, the sensor orientation in space is arbitrary. Therefore, such IMUs are equipped with a set of three orthogonally mounted accelerometers and a similar set of three gyroscopes to allow determination of the full vectors (acceleration and angular rotation) in space. In contrast, a local level platform principally requires only two accelerometers for navigation in the horizontal plane, because the sensors are always horizontally aligned.

As discussed above, equation (1) is only valid in the *i*-frame, where Newton's laws hold. As soon as the vectors refer to a rotating frame, one needs to take into account apparent forces. The frames commonly used in inertial navigation are the earth centred earth fixed frame (*e*-frame of type WGS84) and the local level *l*-frame, which is centred in the vehicle and thus moves with it along the trajectory. Its axes might be defined as pointing east, north and up (ENU-system) or north, east and down (NED-system). Following the derivation in Jekeli (2001), the general formulation of the equation of motion in an arbitrary *n*-frame reads

$$\ddot{\boldsymbol{x}}^n = \boldsymbol{f}^n + \boldsymbol{G}^n - 2\boldsymbol{\Omega}_{in}^n \dot{\boldsymbol{x}}^n - \dot{\boldsymbol{\Omega}}_{in}^n \boldsymbol{x}^n - \boldsymbol{\Omega}_{in}^n \boldsymbol{\Omega}_{in}^n \boldsymbol{x}^n, \tag{2}$$

where again the exponent marks the reference frame and the matrix $\boldsymbol{\Omega}_{in}^n$ (with indices *i* and *n*) contains the rotational rates of the *n*-frame with respect to the *i*-frame, coordinatized in the n-frame (upper index). The last three terms on the right hand side are apparent forces, which only show up in a rotating frame. They can be identified as the Coriolis-, Euler and centrifugal accelerations. The *n*-frame can now be chosen to be either the *i*-, *e*- or *l*-frame. In case of choosing the *i*-frame, the equation reduces to equation (1). In case of the *e*-frame, the matrix $\boldsymbol{\Omega}_{in}^n$ contains the elements of the rotation vector of the *e*-frame around the *i*-frame, which is the earth rotation vector ω_{ie} (one rotation per day). Since the time variations of this vector are too small to be sensed by currently available IMU gyroscopes, the Euler term is neglected (actually gyroscopes measuring variations in Earth rotation have been built (Schreiber et

al., 2004), but they have diameters of several meters and are not used for navigation purposes). Combining the vectors of gravitation and centrifugal acceleration to form the gravity vector $\boldsymbol{g}$, the equation of motion in the *e*-frame finally reads

$$\ddot{\boldsymbol{x}}^e = \boldsymbol{f}^e + \boldsymbol{g}^e - 2\boldsymbol{\Omega}_{ie}^e \dot{\boldsymbol{x}}^e \,. \tag{3}$$

In the *l*-frame the same equation reads

$$\frac{\mathrm{d}}{\mathrm{d}t}\boldsymbol{v}^l = \boldsymbol{f}^l + \boldsymbol{g}^l - (\boldsymbol{\Omega}_{il}^l + \boldsymbol{\Omega}_{ie}^l)\boldsymbol{v}^l \,. \tag{4}$$

Here the first and second time derivatives of the position vector are replaced by the velocity vector $\boldsymbol{v}$ and its first time derivative. This is done, because the *l*-frame is moving with the vehicle and therefore the position vector of the vehicle as well as all time derivatives in the *l*-frame (including $\ddot{\boldsymbol{x}}^l$) are zero by definition. The velocity vector $\boldsymbol{v}^l$ actually represents the *e*-frame velocity in the orientation of the *l*-frame, such that $\dot{\boldsymbol{x}}^e$ is expressed in terms of its north, east and vertical components according to

$$\boldsymbol{v}^l = \boldsymbol{C}_e^l \dot{\boldsymbol{x}}^e \,. \tag{5}$$

In order to derive the state vector from the equations of motion – such as equations (1), (3) or (4) – one needs to integrate the equations in time. This step is carried out in the so called *mechanization equations* (Jekeli, 2001; Schwarz and Wei, 2001; Hofmann-Wellenhof et al. 2003). Figure 1 shows a flow chart of the corresponding computations, as carried out in the *l*-frame. Basically equation (4) is integrated once to determine velocities and twice to determine positions. Input parameters into equation (4) are the measured specific force as well as gravity (determined from a gravity model) and velocity to compute the Coriolis term. Before using the specific force vector in equation (4), the original observations $\boldsymbol{f}^b$ need to be transformed to the *l*-frame. The required transformation matrix contains the current attitude angles of the vehicle and is determined from an integration of the gyro-observed angular rates. The output is the state vector consisting of position, velocity and attitude. These elements also serve as initial conditions for the next integration step. For the first step, the initial conditions need to be determined by way of a static or kinematic (on-the-fly) alignment (Jekeli, 2001; Rogers, 2007).

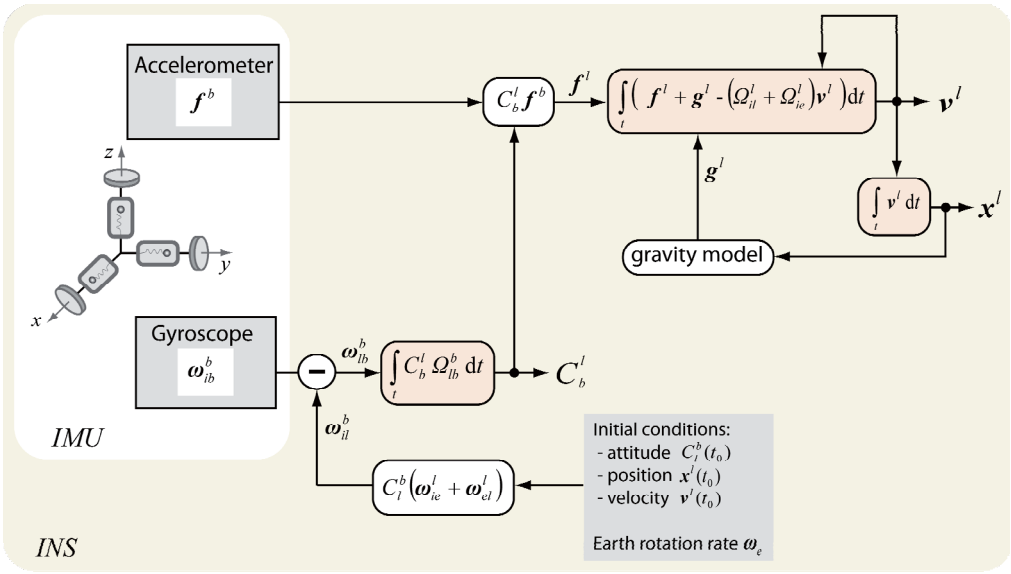

Figure 1: Mechanization equations in the local level frame.

Gravimetry on moving platforms

A gravimeter is a very precise one-axis accelerometer. Working in the l-frame and with $\boldsymbol{v}^l = 0$ (static mode), equation (4) reduces to $\boldsymbol{f}^l = -\boldsymbol{g}^l$, which shows, that in the static case, the accelerometer directly senses gravity and therefore acts as a gravimeter. Putting the accelerometer on a moving platform, one basically needs to take into account the effect of the Coriolis force as given by the last terms in equation (4). In case of static terrestrial gravimetry the instrument is aligned horizontally, i.e. the z-axis of the l-frame is parallel to the plumb line. Then only the vertical component of the gravity vector is different from zero and gravity can be measured by a single accelerometer with sensitive axis along the vertical. This concept can be extended to the kinematic case, provided the gravimeter is mounted on a local level stabilized platform to keep it horizontal and the Coriolis effect is properly taken into account. This method is operationally used in airborne or ship-borne gravimetry (see e.g. Olesen, 2002) using dedicated gravimeters, like e.g. the air/sea gravimeter by LaCoste & Romberg, shown in figure 2. Solving equation (4) for gravity and restricting the equation to the vertical component (pointing downward), the gravity value can be determined by

$$g = \ddot{h} - f_D - \left(2\omega_e v_E \cos\phi + \frac{v_N^2 + v_E^2}{R} \right). \qquad (6)$$

In addition to the readings f_D from the accelerometer (or gravimeter) one needs to know the vertical kinematic acceleration $\ddot{h}$. This can be derived, e.g., from GPS measurements, where attention must be payed to the increase of high frequent noise due to the second order time derivation of the position coordinate. Therefore a proper low-pass filtering is required. This will be discussed later. The term in brackets, representing the sum of Coriolis effect plus the transport rate effect (movement along the curved earth surface), is called the *Eötvös correction* (Jekeli, 2001). It is computed using the horizontal velocities (east and north) derived in the navigation solution.

Figure 2: Air-Sea Gravity System by LaCoste&Romberg, mounted on a dynamically stabilized platform (source: www.microglacoste.com).

Vector gravimetry for geoid profiling

Aligning the l-frame not with the actual plumb line, but with the ellipsoidal normal, the horizontal components of the gravity vector do no longer vanish. They represent the deflections of the vertical and are a measure for the inclination of the geoid with respect to the ellipsoid as shown in figure 3. According to Hofmann-Wellenhof & Moritz (2005) the difference in geoid height between two points is given by

$$\mathrm{d}N = -\varepsilon \, \mathrm{d}s \,, \qquad (7)$$

where ε is the component of the deflection of the vertical in direction of the trajectory and $\mathrm{d}s$ is the horizontal distance. Integrating the geoid height differences along the trajectory gives a geoid profile, which is derived from local data only, see e.g. Schwarz (1987) or Jekeli and Kwon (2002), who report relative geoid accuracy of better than 10 cm over spatial wavelength of 10–20 km. Using gravity values instead of the deflection components, one would need to integrate data from a larger area surrounding the trajectory, to determine the geoid. Measuring all components of the gravity vector, one speaks of *vector gravimetry*, while *scalar gravimetry* (equation 6) is restricted to the vertical component only. A strapdown IMU is capable to act as a vector gravimeter, while the operational air-

borne gravimeters on stabilized platforms are limited to scalar gravimetry.

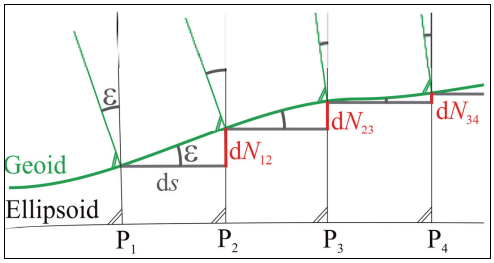

Figure 3: Geoid profiling along the trajectory between points P1 and P4.

The spectral window of airborne gravimetry

In navigation, the strength of the combination of INS and GPS is that both compensate for the weaknesses of the other. While INS is very precise on short time scales, the navigation solution strongly drifts from the true trajectory over long periods due to the integration of systematic errors. In contrast, GPS is stable on the long run, while the precision from epoch to epoch is of lower quality than for INS. The optimal combination makes use of GPS for the low frequencies (long time periods) and INS for the high frequencies. This is qualitatively shown in figure 4 (green line). The combined GPS/INS navigation solution is of high quality over the whole frequency range. This can also be illustrated by considering the individual elements in the equation of motion, e.g. in equation (1). Here the gravitational part is considered to be known from a model of the gravitational field and the specific force is measured. From both, the kinematic acceleration can be computed. In addition it can directly be determined from GPS observations, such, that INS (computed) and GPS (observed) mutually control each other. In contrast, solving the same equation for gravitation,

$$\boldsymbol{b}^i = \ddot{\boldsymbol{x}}^i - \boldsymbol{f}^i \qquad (8)$$

the right hand side contains both the INS and GPS observations. These are subtracted from each other, with no means for mutual control. Therefore the high frequencies in the combined GPS/INS gravimetry solution are dominated by errors in the GPS-accelerations, while the low frequencies are dominated by INS errors, as indicated by the orange line in figure 4. Setting certain requirements for the acceleration accuracy, only a medium frequency band is usable for gravimetry, as illustrated by the yellow band. The upper and lower limits of this band depend on the specific setup and instrumentation of the individual measurement campaign as well as the accuracy requirements (see also Jekeli, 2001).

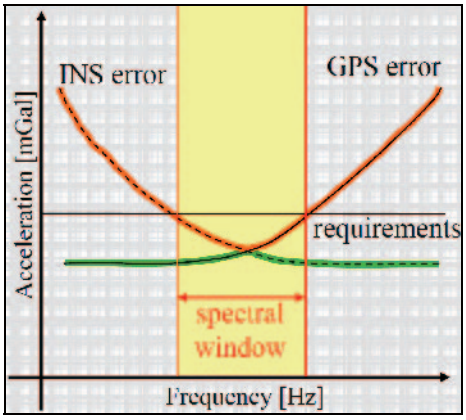

Figure 4: Spectral window of airborne gravimetry. Solid line: GPS derived acceleration errors; dashed line: IMU acceleration errors; green line: error of combined GPS/INS navigation; orange line: error of GPS/INS gravimetry.

Gravity values along a real flight trajectory

In the following, first results achieved at the Geomatics group at UMB in Ås will be presented. The data were obtained during a flight experiment in the German Alps using a navigation grade IMU available at IAPG. Deriving only scalar gravity values, the method is usually referred to as *strapdown inertial scalar gravimetry* (SISG). In future investigations, also the horizontal components will be determined, thus allowing for full vector gravimetry.

Test area and flight trajectory

The experiment was carried out over the Estergebirge mountains (central mountain block in the digital terrain model in figure 6) in the German Alps, about 80 km south of Munich in close vicinity to the city of Garmisch-Partenkirchen. Since several years, IAPG operates a test bed for physical geodesy in Estergebirge, where gravity values, deflections of the vertical and GPS have been measured in high density along with geometric levelling (Flury, 2002). The highest peak of Estergebirge mountains is about 2085m high, while the valley reaches down to about 600m. The area is an ideal test bed, providing dense high quality ground truth data for validation of airborne gravimetry. Figure 6 also shows the flight trajectory of the current experiment. With 2400 m the flight altitude was well above the highest peak. Travelling on an average speed of about 50 m/s, the mission duration was about 2 hours. Several cross-points along the trajectory allow for internal consistency checks.

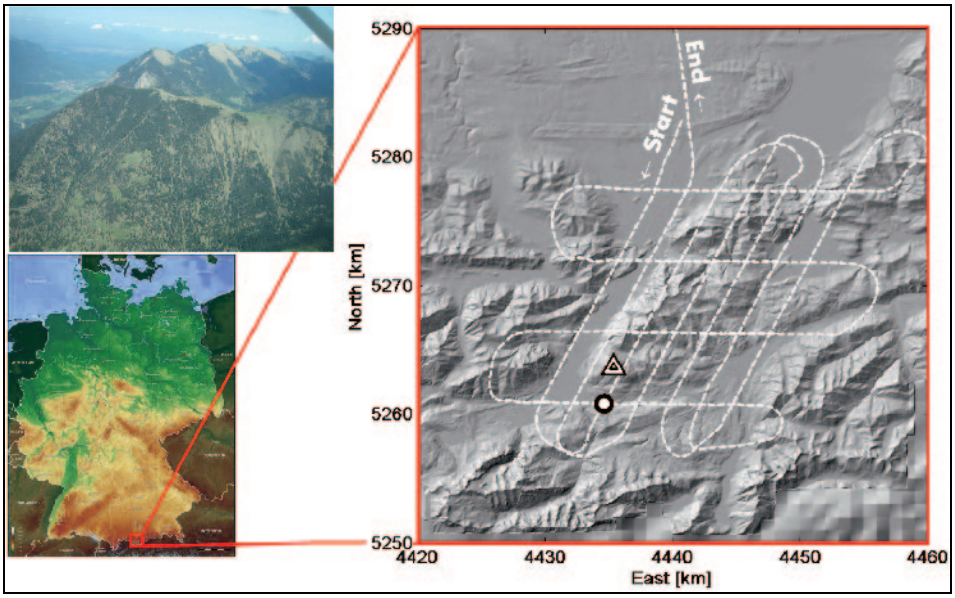

Figure 5: Test area of Estergebirge mountains in the German Alps.

Instrumentation

The instrumentation used in the experiment was provided by IAPG and BEK. The iNAV-RQH IMU is a navigation grade instrument developed by the German company iMAR (see www.imar-navigation.de) and carries an orthogonal triad of QA2000-40 selected accelerometers and a similar triad of GG1320 ring laser gyroscopes (both sensor types manufactured by Honeywell). The main performance characteristics of the inertial sensors as given by the manufacturer are listed in table 1. The IMU was installed in a 4-seat Cessna 172 aircraft, next to the pilot (with the co-pilot seat being removed; see photograph in figure 6). On top of the aircraft (almost right above the IMU) a GPS antenna was mounted and connected to a 20 Hz L1/L2 Novatel GPS receiver. In order to refer the IMU and GPS results to a common reference point, the position vector between the two, the so called lever arm, had to be determined. Measuring distance and directions with a total station (see photograph in figure 7), the position of the GPS antenna was obtained in the IMU body-frame.

Table 1: Performance characteristics of GG1320 gyroscopes and QA2000 accelerometers.

	Gyroscope	**Accelerometer**
Measurement range	*± 500 deg/s*	*± 2 g*
Resolution	*1.13 arcsec*	*0.2 µg*
Non-linearity	*10 ppm*	*15 µg/g²*
Scale factor error	*10 ppm*	*70 ppm*
Angular random walk	*0.0018 deg/√Hz*	–
Acceleration noise density	–	*8 µg/√Hz*
Bias repeatability	*0.002 deg/h*	*< 15 µg*

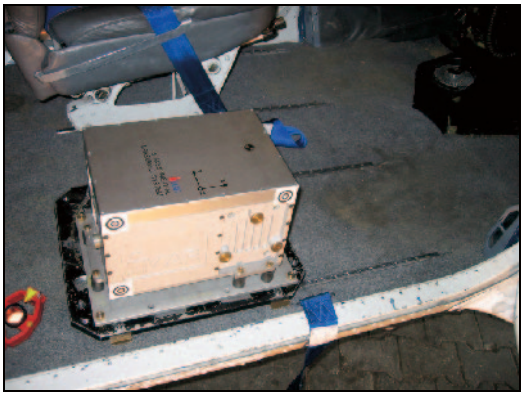

Figure 6: The iNAV-RQH inertial measurement unit installed in the plane.

Figure 7: Tachymetric determination of the lever arm between IMU and GPS antenna.

GPS accelerations

The kinematic accelerations of the aircraft, i.e. the vector $\ddot{\boldsymbol{x}}$ as given in the equations of motion (1)–(4) or in case of scalar gravimetry the vertical component $\ddot{h}$ in equation (6), were derived from a differentiation of the time series of GPS positions. The positions can be determined both by relative GPS with respect to a base station (DGPS) or by absolute positioning using the precise point posi-

tioning (PPP) method (see e.g. Zumberge et al, 1997; Kouba and Heroux, 2001; Øvstedal, 2002; or Øvstedal et al. 2006). For the derivations of kinematic accelerations, the PPP-solution, provided by the software package TerraPos (Kjørsvik, 2006), was used. The corresponding time series of positions is very smooth due to forward and backward filtering. In contrast, the DGPS solution obtained from the software package Kingspad[1] (Schwarz and El-Sheimy, 2000), developed at the University of Calgary, uses forward filtering only, which can lead to jumps or small discontinuities (e.g., when the satellite constellation is changing, or in case of cycle slips). Therefore it was more convenient to derive accelerations from the smooth PPP solution.

For the differentiation, a FIR differencing filter (see e.g. Bruton et al., 1999) of order 68 was used, which takes derivatives in the spectral domain. Since an ideal filter cannot be constructed, the actual differentiator also filters out part of the high frequencies, as shown in the frequency response plot in figure 8. There the frequency axis is labelled with relative values, where 1 stands for the highest frequency, the Nyquist frequency, which is half the sampling frequency. The TerraPos solution was generated at a 5 Hz sampling. Therefore the Nyquist frequency is 2.5 Hz and accelerations derived from the FIR differentiator contain the full signal up to about 2 Hz, while damping higher frequencies. In general such low-pass filtering of the accelerations is advantageous, because the position noise in the high frequencies is strongly amplified by differentiation. Since the 5 Hz signal still contains too much high frequent noise, the gravity values derived from equation (5), i.e. the difference between GPS-derived and IMU-observed accelerations, need further low-pass filtering. The corresponding increase in signal strength of the original gravity signal (denoted by SISG) is clearly visible in figure 10 for components above 70 seconds period.

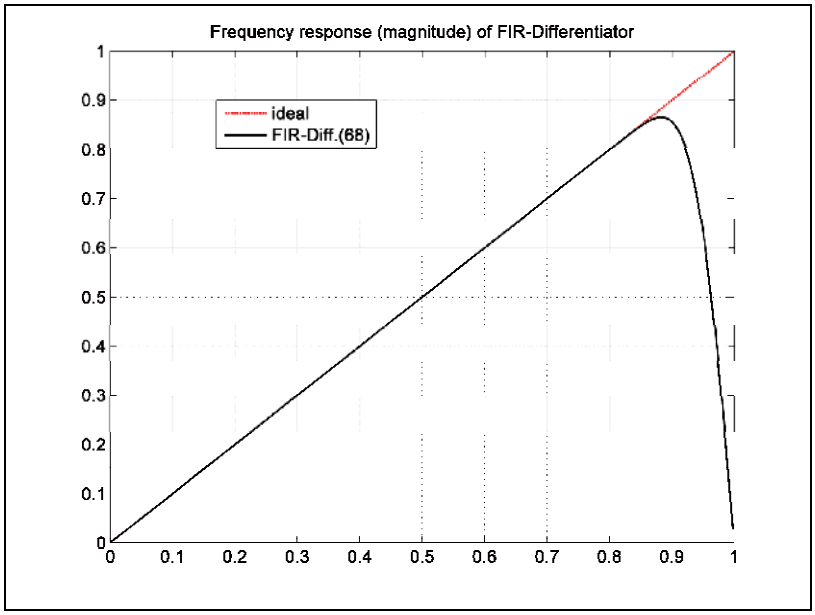

Figure 8: Magnitude response of ideal and implemented differentiating filter.

1. Kingspad is a dedicated navigation software which uses a Kalman filter with 15 state variables to determine an optimal combined GPS/INS navigation solution. The software is available at IAPG.

IMU accelerations

Before applying equation (6), the raw IMU observations, given at 200 Hz intervals, need to be sampled at the same epochs as the GPS accelerations. In order to avoid aliasing effects, the time series of the specific force vector was low-pass filtered and decimated to 5 Hz sampling. For low-pass filtering a zero-phase forward and reverse FIR filter was used.

Data processing overview

Applying now equation (5) to derive gravity values, the specific force vector needs to be transformed from the b-frame to the l-frame and the GPS observations must be referred to the same reference point as the IMU data, i.e. the velocity and acceleration effect on the lever arm must be subtracted from the GPS derived velocities and positions. The orientation of the aircraft was determined from a combined GPS/INS navigation solution as provided by the Kingspad software. The computations correspond to the mechanization equation flow-chart in figure 1. The whole processing chain is shown in figure 9. Since Kingspad makes use of DGPS rather than PPP, a station of the German DGPS reference station network SAPOS was used. The location of this station is indicated with a triangle in figure 5.

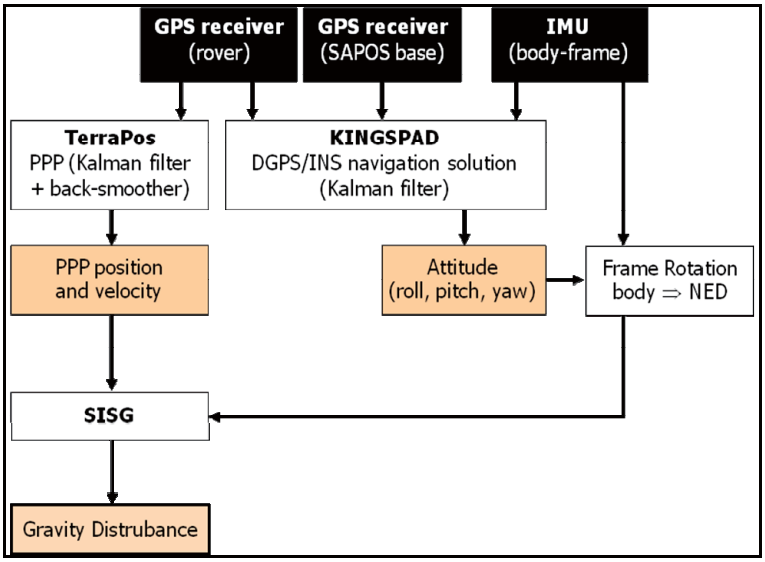

Figure 9: Processing chain of the airborne gravimetry experiment.

Subtracting normal gravity γ from the gravity values derived according to equation (6), a time series of gravity disturbances δg was determined (still with 5 Hz sampling). Being strongly contaminated by high frequency noise above 0.014 Hz (as shown in figure 10), which corresponds to about 70 seconds, this time series was further low-pass filtered down to about 70 seconds. Considering the speed of 50 m/s, this corresponds to a spatial resolution (half wavelength) of about 2 km. In addition to the 70 seconds period, also 2 hours (corresponds to the mission duration) and 6 minutes (corresponds to the average length of one leg of the trajectory) periods are marked in figure 10. The figure does not show a drift in the SISG results, which would lead to increased signal strength in the low frequencies. It can therefore be assumed, that the bias stability of the accelerometers does not affect the results during the mission duration.

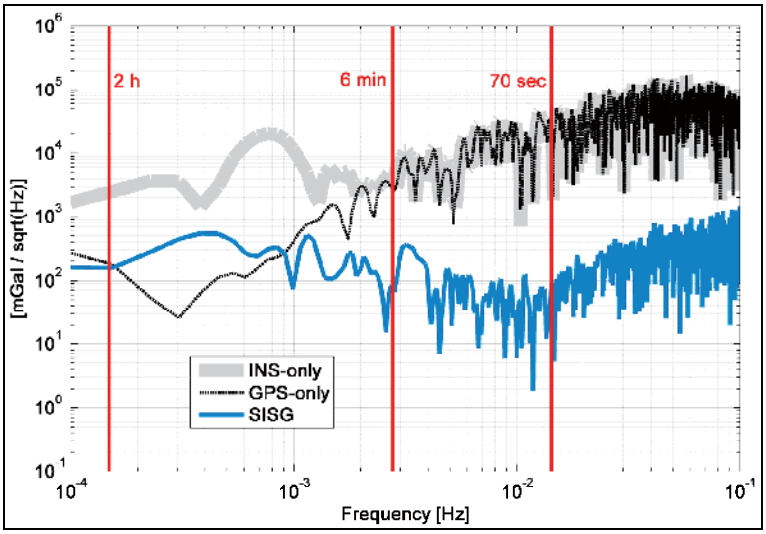

Figure 10: Spectrum of accelerations from INS, GPS and strapdown inertial scalar gravimetry (SISG).

Gravity disturbances along the flight track

The final result is shown in figure 11 as time series of δg plotted against topographic heights (topographic masses should be the dominating component in δg) as well as in figure 12, where the same result is plotted in space along with a shaded relief of the topography. As figure 11 reveals, the results from airborne gravimetry fit very well to the topographic signal, which is a first indication for the quality of the results. In order to quantify the internal consistency of the results, the values of δg along different sections of the trajectory were compared at cross over points. Figure 12 shows that the values fit quite well at these crossings and the RMS of the differences is at the level of 5 mGal. It must be considered however, that the signal is low-pass filtered in time, i.e. along the trajectory. Therefore an east-west leg will never match perfectly with a north-south leg, except for very smooth signals. In case the signal structure is very an-isotropic, i.e. the signal behaviour strongly depends on direction, the misfit at cross-overs will rise. One such point is indicted in figure 6 (circle), where the signal along the east-west leg is parallel to a valley and therefore there are no strong signal variations, while the north-south leg leads across the valley, such that the signal varies strongly. The misfit at this point is 15 mGal. Not considering those two points, which show the largest misfit (13 and 15 mGal), the overall RMS is reduced from 5 mGal to 3 mGal. This is a more realistic measure for the internal consistency of the results. In a further step, the topographically induced signal will be reduced from the gravity disturbances. This way the signal gets smoother and the misfit due to direction dependent filtering can be expected to decrease.

Outlook for future investigations

As has been shown in this first experiment, it is possible to derive gravity with a spatial resolution of some few kilometres and a precision of about 3 mGal using a navigation grade strapdown IMU. This is about the same level of accuracy, as achieved by Bruton (2000), Schwarz and Li (2000), Wei and Tennant (2001) or Kwon and Jekeli(2001), who report about 2–4 mGal for spatial resolutions between 2 and 5 km. The result is also com-

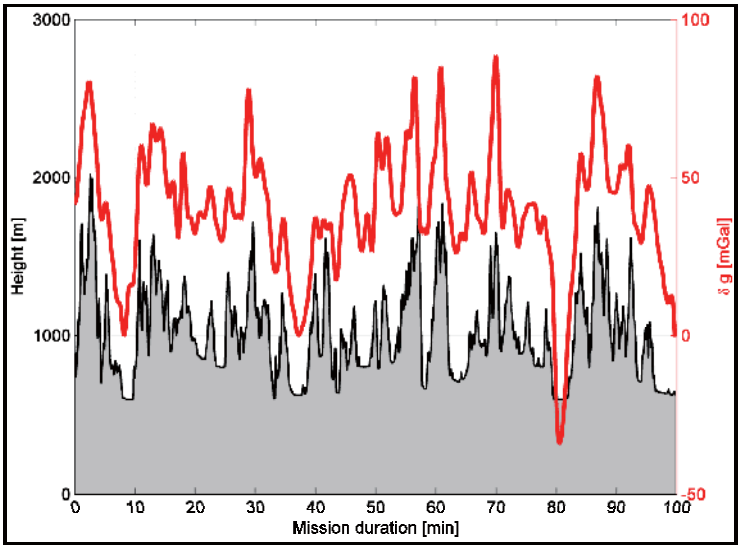

Figure 11: Time series of SISG results and topographic heights along the trajectory.

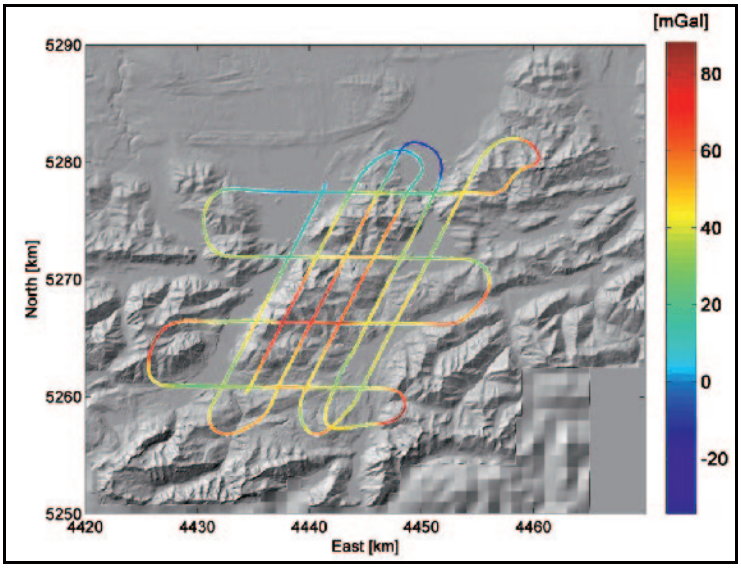

Figure 12: Color-coded geographic representation of SISG results along the trajectory.

parable to airborne gravimetry using conventional gravimeters on a stabilized platform, where about 2 mGal are reported for resolutions of about 5–6 km (Olesen et al., 2002). Furthermore, the strapdown instrumentation allows for direct geoid profiling using the horizontal components from vector gravimetry, as shown already by Jekeli and Kwon (2002). This way the integration of gravity over larger areas can be avoided, when only local information is desired from airborne gravimetry. It must be considered, however, that the geoid profile gives only differences along the trajectory, and not absolute values. The processing of the horizontal components is not implemented yet, but it will be the next step in the analysis of the flight campaign.

Acknowledgements GPS data of the reference station at mount Wank were provided by Dr. Völksen of BEK, which is gratefully acknowledged.

References

Bruton, A. M., C. L. Glennie, K. P. Schwarz (1999) Differentiation for high precision GPS velocity and acceleration determination. *GPS Solutions,* 2(4), pp. 7–21.

Bruton A.M. (2000) Improving the accuracy and resolution of SINS/DGPS airborne gravimetry. UCGE report 20145, Department of Geomatics Engineering, University of Calgary.

ESA (1999) Gravity field and steady-state ocean circulation mission. Reports for mission selection: The four candidate earth explorer core missions, SP-1233(1).

Flury J. (2002) Schwerefeldfunktionale im Gebirge. DGK C, 557, Verlag der Bayerischen Akademie der Wissenschaften, Munich, Germany.

Glennie C.L. (1999) An analysis of airborne gravity by strapdown INS/GPS. UCGE report 20125, Department of Geomatics Engineering, University of Calgary.

Hofmann-Wellenhof B. and H. Moritz (2005) Physical Geodesy. Springer.

Hofmann-Wellenhof B., K. Legat, M. Wieser (2003) Navigation. Springer, Wien.

Jekeli Ch. (2001) Inertial Navigation Systems with Geodetic Application. Walter de Gruyter, Berlin.

Jekeli Ch. and J.H. Kwon (2002) Geoid profile determination by direct integration of GPS inertial navigation system vector gravimetry. *Journal of Geophysical Research*, Vol. 107, No. B10, 2217, doi:10.1029/2001JB001626.

Kjørsvik N.S. (2006) TerraPos – User manual. Terratec AS, Norway.

Kouba J., P. Heroux (2001) Precise Point Positioning using IGS orbit and clock products. *GPS Solutions*, 5(2): 12–28.

Kwon J.H. and Ch. Jekeli (2001) A new approach for airborne vector gravimetry using GPS/INS. *Journal of Geodesy*, 74: 690–700.

NIMA (2002) The American Practical Navigator. National Imagery and Mapping Agency, Maryland.

Olesen A.V., R. Forsberg, K. Keller, A.H.W. Kearsley (2002) Error sources in airborne gravimetry employing a spring-type gravimeter. In: Ádám and Schwarz (eds.) Vistas for Geodesy in the new millenium. IAG Symposia, Vol. 125, Springer.

Rummel R., Balmino G., Johannesen J., Visser P., Woodworth P. (2002) Dedicated gravity field missions – principles and aims. *J Geodynamics*, 33:3–20.

Rogers R.M. (2007) Applied Mathematics in Integrated Navigation Systems. AIAA Education Series.

Schreiber U., A. Velikoseltsev, M. Rothacher, T. Klügel, G.E. Stedman, D.L. Wiltshire (2004) Direct measurement of diurnal polar motion by ring laser gyroscopes. *J. Geophys. Res.*, Vol. 109 No. B6, doi:10.1029/2003JB002803, B06405.

Schwarz K.P. (1983) Inertial Surveying and Geodesy. *Reviews of Geophysics and Space Physics*, Vol. 21, No. 4, 878–890.

Schwarz K.P. (1987) Geoid profiles from an integration of GPS satellites and inertial data. *Boll. Geofis. Teorica Appl.*, 2, 117–137.

Schwarz K. P. and N. El-Sheimy (2000) Kingspad User Manual – Version 3.0. Department of Geomatics Engineering, University of Calgary.

Schwarz K.P. and M. Wei (2001) INS/GPS integration for geodetic applications. Lecture Notes ENGO 623, Department of Geomatics Engineering, University of Calgary.

Schwarz K.P. and Y.C. Li (2000) Accuracy and Resolution of the Local Geoid Determined from Airborne Gravity Data. IAG Symposia, Vol. 123, Springer.

Tapley B.D., Ch. Reigber (1999) GRACE: A satellite-to-satellite tracking geopotential mission. *Boll. Geofis. Teorica Appl.*, 40(3–4), 291.

Torge W. (1991) Geodesy. Walter de Gruyter, Berlin.

Wei M. and J.K. Tennant (2001) STAR-3i Airborne Gravity and Geoid Mapping System. IAG Symposia, Vol. 123, Springer.

Zumberge J., M. Heflin, D. Jefferson, M. Watkins, F. Webb (1997) Precise point positioning for the efficient and robust analysis of GPS data from large networks. *J. Geophys. Res.*, 102(B3), 5005–5017.

Øvstedal O. (2002) Absolute Positioning with Single Frequency GPS Receivers. *GPS Solutions*, 5(4): 33–44.

Øvstedal O., J.G.O. Gjevestad, N.S. Kjørsvik (2006) Surveying using GPS Precise Point Positioning. Paper presented at the XXIII. FIG Congress, Munich, Germany, October 8–13, 2006.